Increasing Wind-Driven Wildfire Risk Across California's Sierra Nevada Mountains

Callum Thompson[1], Charles Jones[2], Leila Carvalho[3], Anna Trugman[3], Donald D Lucas[4], Daisuke Seto[3], and Kevin Varga[1]

[1]University of California, Santa Barbara
[2]University of California Santa Barbara
[3]University of California, Santa Barbara
[4]Lawrence Livermore National Laboratory

November 24, 2022

Abstract

Surface winds are an important factor in wildfire growth and the decision-making process of when utility companies shut off power to suppress fire ignitions. However, long-term trends in surface winds and their implications for fire weather have received less attention compared to trends in temperature, humidity, and precipitation. This article uses the ERA5 reanalysis to calculate surface wind trends over California during 1979–2019. We find statistically significant increases in surface easterlies during autumn on the western slopes of the Sierra Nevada Mountains and increases in Hazardous Wind Events of heightened wind-related fire risk. Using the Canadian Fire Weather Index, we also show that wildfire risk has mainly increased over the Sierra Nevada Mountains, indicating that strengthening winds has contributed to a growing risk of wind-driven wildfires in this region compared to 40 years ago.

Increasing Wind-Driven Wildfire Risk Across California's Sierra Nevada Mountains

Callum Thompson[1], Charles Jones[1,2], Leila Carvalho[1,2], Anna Trugman[1,2], Donald D. Lucas[3], Daisuke Seto[1] and Kevin Varga[1]

[1]Earth Research Institute, University of California Santa Barbara
[2]Department of Geography, University of California Santa Barbara
[3]Lawrence Livermore National Laboratory

Key Points:

- Surface easterly downslope wind speeds have increased on the western slopes of the Sierra Nevada Mountains.
- Increased easterly downslope wind speeds have contributed to more frequent events of wind-related fire risk.
- California has become increasingly exposed to extreme fire weather conditions, as measured by the Canadian Fire-Weather Index.

Corresponding author: Callum Thompson, `callum-thompson@ucsb.edu`

Abstract

Surface winds are an important factor in wildfire growth and the decision-making process of when utility companies shut off power to suppress fire ignitions. However, long-term trends in surface winds and their implications for fire weather have received less attention compared to trends in temperature, humidity, and precipitation. This article uses the ERA5 reanalysis to calculate surface wind trends over California during 1979-2019. We find statistically significant increases in surface easterlies during autumn on the western slopes of the Sierra Nevada Mountains and increases in Hazardous Wind Events of heightened wind-related fire risk. Using the Canadian Fire Weather Index, we also show that wildfire risk has mainly increased over the Sierra Nevada Mountains, indicating that strengthening winds has contributed to a growing risk of wind-driven wildfires in this region compared to 40 years ago.

Plain Language Summary

Surface winds in California are an important factor in wildfire growth and are one criterion by which utility companies decide whether to shut off powerlines in order to mitigate fire risk. However, long-term changes in surface winds have received less attention in comparison to changes in temperature, humidity, and rainfall. In this article, we use a new weather and climate dataset with a resolution of 31 km to investigate how surface winds have changed over California from 1979 to 2019. We find that wind speeds have distinctly increased on the western slopes of the Sierra Nevada Mountains associated with downslope winds from the east, and that there has been more frequent periods of strong, dry northeasterly winds. Over the same time period, wildfire risk has increased most over the Sierra Nevada Mountains, indicating that stronger winds have contributed to a growing risk of wind-driven wildfires in this region compared to 40 years ago.

1 Introduction

Over the past 20 years, California has seen a marked increase in burned forest area, during which time 11 of the 20 largest wildfires in the state's history have occurred (Table S1) (OES, 2018; CalFire, 2020b). Concurrently, recent wildfire seasons have also incurred substantial damage to property and loss of life, with 17 of the 20 most destructive wildfires also occurring during this period (Table S2) (CalFire, 2020a). This increased frequency of large and destructive wildfires has often been attributed to a combination of increasing temperatures (Hayhoe et al., 2004; Hughes et al., 2011; Williams et al., 2019), decreasing humidity (Hughes et al., 2011), drier fuels (Williams et al., 2019), earlier spring snow melt (Westerling et al., 2006), and a later onset of autumn precipitation (Goss et al., 2020).

However, high wind speeds are an additional critical factor driving extreme fire weather conditions. For California, high winds typically occur as downslope Foehn winds during fall and winter, originating from high pressure systems in the Great Basin that direct winds towards the U.S. west coast (Jones et al., 2010; Abatzoglou et al., 2013; Werth et al., 2016; Brewer & Clements, 2020). Over Northern California and the Sierra Nevada Mountains, these winds are usually called Diablo winds and over Southern California are known as Santa Ana winds. Sundowner winds over Santa Barbara also share many characteristics of Diablo and Santa Ana winds, but are more frequent during spring, are strongly tied to the diurnal cycle of radiative surface energy input, and are typically associated with pressure gradients conducive to north—south flow over the Santa Ynez Mountains (Hatchett et al., 2018; Duine et al., 2019; Carvalho et al., 2020; Jones et al., 2021). Despite these regional differences, these strong winds have each played a devastating role in many of California's most infamous wildfires by damaging powerlines and rapidly fanning the resulting fire. Santa Ana and Sundowner winds fanned the Thomas Fire (2017) which burned 281,893 acres, the largest fire in California's history at the time (Fovell & Gallagher, 2018; Kolden & Henson, 2019). In the same year, the Tubbs Fire (2017) burned 36,807 acres over a month that saw hurricane-force Diablo winds and subsequently became the most deadly wildfire in the state's history (Nauslar et al., 2018; Coen et al., 2018). However, this record was again broken the next year when Diablo winds incited the Camp Fire (2018), burning 70,000 acres in 24 hours and 153,336 acres in total (Brewer & Clements, 2020; Mass & Ovens, 2021). The alarming rate at which these devastating wind-driven wildfires has occurred raises the question of how surface winds have changed over recent decades. Furthermore, Public Safety Power Shutoffs (PSPSs), whereby utility companies shut off power lines during periods of heightened fire risk, incorporate wind speed as one criterion when determining fire risk (Abatzoglou et al., 2020). This societal aspect provide additional motivatation to analyze changes in surface winds, not just to better understand the changing meteorological landscape, but to better inform PSPS practices, too.

Despite the urgency to better understand changes in the wind landscape and wind-driven fire events, however, such studies are relatively sparse and a state-wide picture is yet to emerge. In one study, Liu et al. (2020) found no discernible trend in either Diablo maximum wind speeds or frequency in the ERA5 reanalysis over the San Francisco Bay. For Southern California, Guzman-Morales et al. (2016) described a modest increase in Santa Ana wind intensity during 1948-2012, while Rolinski et al. (2019) reported a marked increase in Santa Ana wind frequency after 2007 in a downscaling of the North American Regional Reanalysis (NARR). Yet, one region where trends in wind speed and high wind events remains unexamined is the Sierra Nevada Mountains, despite its expanding wildland-urban interface risking further fire-related societal cost (Hammer Roger B. & I., 2007; Mass & Ovens, 2021).

Therefore, to build a state-wide picture of changing surface winds over California we address three questions in this study: 1) Where are wind speed trends changing significantly?; 2) What are the wind direction trends associated with wind speed trends?; 3) Where has the frequency of high wind events changed significantly? These trends were calculated for the most occurrent wildfire months of June-July-August (JJA) and September-October-November (SON) over 1979–2019 using the ERA5 reanalysis (Hersbach et al., 2020). ERA5 has a grid spacing of approximately 31 km x 31 km, is the first reanalysis with hourly output, and includes the Canadian Fire Weather Index as a reanalysis variable, one of the most sophisticated metrics of fire weather risk used operationally worldwide (Field et al., 2015; Vitolo et al., 2020). Using ERA5, we analyzed trends in wind speed, wind direction, high wind events, and the Fire Weather Index to elicit the role of surface winds in contributing to California's evolving wildfire landscape. This analysis is presented in the rest of this article as follows: section 2 details the methods of how trends in wind speed, wind direction and high wind events were calculated, section 3 presents trends in wind speed (section 3.1), wind direction (section 3.2), Hazardous Wind Events (section 3.3), and wildfire conditions (section 3.4). Finally, conclusions are summarized in section 4.

2 Data and Methods

In this study, we used the ERA5 reanalysis which has a native grid spacing of approximately 31 km. Although this grid spacing is still too coarse to accurately resolve winds over local complex topography, ERA5 is still well correlated with observed winds over complex terrain (> 0.77), captures the diurnal cycle well, and most closely resembles the observed interannual variability compared to four other reanalysis products (Ramon et al., 2019; Jourdier, 2020). Therefore, despite its resolution restrictions, ERA5 is still well suited to an analysis of long-term wind speed trends.

These trends were calculated from the reanalysis as follows: hourly 10-meter zonal and meridional wind components were used to calculate the 10-meter wind speed during 1979–2019 for JJA and SON. Seasonal averages of daytime (0600–1700 PST) maximum winds and night-time (1800–0500 PST) maximum winds were then calculated at each grid point with linear trends in these seasonal averages calculated using the Theil-Sen estimator with statistical significance determined with Mann-Kendall testing at the 95% level (Wilks, 2011).

To elicit the wind direction associated with wind speed trends, we also calculated daytime and night-time trends in zonal and meridional wind components. These components were separated by their positive and negative directions to determine trends in northerly, southerly, westerly, and easterly winds, calculated here as trends in seasonal averages of daily maximum southerly and westerly winds, and in seasonal averages of daily minimum northerly and easterly winds. Trends and their significance were again determined using the Theil-Sen estimator and Mann-Kendall testing.

To examine how winds have changed year-to-year in historically fire prone regions of California, time series in seasonal averages of daily maximum winds were calculated for the following three regions: Northern California (39–41.5 N and 120.5–123.5 W), the Sierra Nevada Mountains (36.25–38.5 N and 117.5–120 W), and Southern California (32.7–35 N and 115–119 W). These regions were chosen due to their wind trends, historical proneness to wildfires, and representativeness of distinct vegetation types that are critical in determining wildfire behavior (Williams et al., 2019). For each region, daily maximum winds above 304 m (1000 ft) were extracted to emphasize winds over complex terrain and averaged for each season over 1979–2019 to construct the time series. Time series were then subtracted from their 1979–2019 average to get the anomaly with trends calculated using the Theil-Sen estimator.

Furthermore, to determine whether there has been a change in the frequency of high wind events associated with heightened wind-driven fire risk, we investigated the frequency of Hazardous Winds Events (HWE) associated with two relevant wind systems affecting California: Santa Ana and Diablo winds. Since both wind regimes are associated with strong, dry northeasterly winds, a HWE was defined at each grid point when

1. the 10-m hourly wind speed was above the 1979–2019 75th percentile wind speed;
2. the 10-m wind direction (calculated from 10-m zonal and meridional winds) was from the northeast quadrant (i.e., 0–90°);
3. the 2-m relative humidity was below the 1979–2019 25th percentile relative humidity;
4. these conditions persisted for at least 6 h;
5. events were separated by at least 12 h.

We chose percentile-based thresholds over fixed-limit thresholds for the wind and humidity criteria, as ERA5 underestimates wind speeds over complex terrain (Jourdier, 2020) and so may not resolve typical Diablo and Santa Ana wind speeds. Using percentile-based criteria for winds and humidity permits 'strong' winds to be defined relative to what the reanalysis can represent and dry conditions to be defined relative to the local climate. Similar criteria have been used to characterize Diablo and Santa Ana winds (Guzman-Morales & Gershunov, 2019; Liu et al., 2020) and, for the criteria used here, monthly averages of the number of HWE within California over 1979–2019 produced the expected seasonal cycle with a HWE peak over autumn and winter (Figure S1). Additionally, time series for regions showing significant HWE trends were calculated by averaging the number of HWE within each region for a given season during 1979–2019. Time series were then standardized by subtracting their average and dividing by their standard deviation to illustrate trends in above- and below-average seasons in the number of HWE.

Finally, wind trends were put in the context of California's changing wildfire risk by calculating trends in the Canadian Fire-Weather Index (FWI) (Field et al., 2015; Vitolo et al., 2020). This index aggregates temperature, relative humidity, 24-hour precipitation, and wind speed, as well as forest-floor moisture to quantify wildfire risk. Fire Weather Indices greater than 30 are considered "Extreme" and are described qualitatively by the Canadian Wildland Fire Information System as "Fast-spreading, high-intensity crown fire, very difficult to control. Suppression actions limited to flanks, with only indirect actions possible against the fire's head." (Field et al., 2015) and references therein). The ERA5 FWI therefore provides a near all-encompassing assessment of wildfire risk and was used to identify where this risk has changed most over California.

3 Results

3.1 Trends in Wind Speed

During JJA we found daytime increasing wind speeds in the Central Valley and Mojave Desert and decreasing winds speeds across the Mendocino Range in northern California (Figure 1a). Significant decreasing winds speeds were also found over the Southern California Bight throughout JJA and SON and were insensitive to the diurnal cycle. (Figure 1a,b,c,d). Instead trends during JJA were more sensitive to the diurnal cycle over land, with widespread significant increasing wind speeds at night over southern California, the Sierra Nevada Mountains (and indeed much of the Intermountain West) (Figure 1b).

Increasing wind speeds over the Sierra Nevada Mountains were even more prominent during SON when they span a narrow corridor on the mountains' western slopes (Figure 1c,d). Trends here highlighted a strengthening of approximately 0.7 m s^{-1} in night-time winds over the total 41-year period (Figure 1d). Furthermore, wind speed distributions were collated at grid points with statistically significant trends between 38.5–36.25 N and 117.5–120.5 W during 1979–1998 and 1999–2018; these distributions showed that the 50th percentile wind speed increased by 4.4%, the 95th percentile increased by 3.1%, and there was an overall higher probability of 1–4 m s^{-1} winds (Figure S2). Although increases are most apparent for weaker winds, changes in stronger winds may be underestimated due to the ERA5's underestimation of winds over complex terrain (Jourdier, 2020). Still, the reanalysis indicates a robust trend towards stronger winds over the Sierra Nevada Mountains where there is a growing wildland-urban interface and where high-elevation wildfires have become increasingly frequent (Schwartz et al., 2015; Alizadeh et al., 2021).

To examine how wind speeds have changed year-to-year, time series in anomalies of seasonally averaged daily maximum winds were also constructed for Northern California, the Sierra Nevada Mountains, and coastal Southern California. Over Northern California, wind speed changes were not statistically significant and tended toward below-average wind speeds during JJA and toward above-average winds during SON (Figures S3a,b), particularly from the early 2000s during SON. Over the Sierra Nevada Mountains, we find little change in maximum wind speeds during JJA (Figure S3c), but a statistically significant increase during SON (Figure S3d), again with a shift toward above-average seasons from the early 2000s. Although there is no statistically significant trend in maximum wind speeds for Southern California, six successive summers of above-average winds occurred over 2014–2019 and five successive autumns of above-average winds over 2015–2019 (Figure S3e,f). Such successive periods of year-on-year high winds increase the risk of wind-driven fires by expediating structural fatigue in powerlines and the surrounding vegetation (Mitchell, 2013).

3.2 Trends in Wind Direction

During JJA, weaker daytime maximum winds seen over the Mendocino Range were associated with a significantly weaker southwesterly flow (Figure 2b,c,g), winds that climatologically prevail over northwestern California (Figure S4a). Trends elsewhere during JJA generally indicated a strengthening of the climatological summer winds, with enhanced westerlies over the Mojave Desert (Figures 2c,g) and enhanced northwesterly flow in the Central Valley (Figures 2a,c,e,g). During SON, we also found northerlies strengthened over the Sacramento Valley (Figure 2i,m) and easterlies strengthened over northeastern and southern California (Figure 2l,p). That these trends have also been found at 80-m in NARR winds (Holt & Wang, 2012), a reanalyis with an identical resolution to ERA5, lends credence to their veracity.

Wind component trends further revealed an amplification of diurnal mountain winds throughout JJA and SON. On the western slopes of the Sierra Nevada Mountains, upslope westerlies strengthened during the day (Figure 2c,k), while downslope easterlies strengthened at night (Figures 2h,p), most prominently where the slopes are steepest in the south of the range. A similar enhancement of diurnal mountain winds is also seen during SON on the western slopes of the Mendocino Range in northwest California (Figures 2k,p). Such an amplification is symptomatic of the snow-albedo feedback whereby increased snowmelt enhances differential heating between the mountains' lower and upper slopes, strengthening upslope flow during the day, followed by radiative cooling and strengthening downslope flow at night. This process has been demonstrated in numerical downscaling experiments for the Himalaya Mountains (Norris & Cannon, 2020) and in upslope winds over the Rocky Mountains (Letcher & Minder, 2017b, 2017a). However, strengthening easterlies may also be related to increasing mean sea level pressure (MSLP) found over the Great Basin and decreasing MSLP over coastal California, favoring southwesterly synoptic winds (Figure S5). Further examination beyond the scope of this study is, therefore, required to disentangle the synoptic- vs local-scale physical mechanisms driving these trends.

Another prominent trend identified was in stronger northerly flow (Figure 2a,e,i,m) associated with the climatological California coastal jet (Figure S4) adjacent to stronger southeasterly flow in the Southern California Bight (Figures 2j,l,n,p). This pattern indicates an enhancement of the Catalina Eddy, a local cyclonic circulation whose causes are still debated, but have been attributed to mountain waves over the San Rafael Mountains creating a north–south pressure gradient over the bight (Bosart, 1983), and convergence from onshore and offshore flow creating positive vorticity that is advected from the north (Kanamitsu et al., 2013). The eddy is typically characterized by a cool marine boundary layer with low cloud and fog which can aid fire suppression (Thompson et al., 1997), indicating another way in which wind trends may have influenced fire weather conditions.

3.3 Trends in Hazardous Wind Events

Trends in wind direction revealed a marked increase in easterlies over much of northeastern California, the Sierra Nevada Mountains in particular, and southern California. As these easterlies are suggestive of downslope Diablo and Santa Ana winds, we investigated whether Hazardous Wind Events have changed significantly over recent decades. Hazardous Wind Events were defined as strong, dry, northeasterly winds lasting at least 6 h, where 'strong' is defined as a wind speed above its grid point 75th percentile wind speed and 'dry' is defined as a relative humidity below its grid point 25th percentile relative humidity.

HWE trends were largely negligible over northern California during both JJA and SON (Figures 3a,b), consistent with Liu et al. (2020), who investigated Diablo wind trends in the ERA5 under similar criteria. However, significant increasing trends were found on the western slopes of the Sierra Nevada Mountains and have occurred more frequently since the early 2000s (Figure 3c), with the autumn of 2018 standing out as a particularly above-average season which also saw the Camp Fire (2018). Additionally, HWE increased significantly over coastal southern California across the Transverse Ranges and Santa Ana Mountains with a marked uptick after 2006 (Figure 3b,d). Although this result was somewhat surprising given the relatively weaker albeit significant wind trends in this region, Rolinski et al. (2019) reported a remarkably similar result in a climatology of Santa Ana winds. However, given the emerging consensus for Santa Ana wind frequency to steadily decline over the 21st century (Miller & Schlegel, 2006; Hughes et al., 2011; Li et al., 2016; Guzman-Morales & Gershunov, 2019) the uptick in Santa Ana winds after 2006 observed here may only represent natural variability rather than a long-term trend. Furthermore, given the relatively weaker wind speed trends over coastal Southern California, we suspect a drying trend has substantially contributed to increases in HWE.

To elicit the effect of long-term drying, we varied the definition of a Hazardous Wind Event, dropping one-at-a-time the wind speed, relative humidity, and wind direction criteria. That is, by considering independently events of 1) strong, dry winds, 2) strong, northeasterly winds, and 3) dry, northeasterly winds (Figures S6–8). Trends over coastal Southern California were particularly sensitive to these criteria, appearing only when all three conditions were included. However, over the Sierra Nevada Mountains, trends remained statistically significant in each case with only some variation in the latitudinal extent of significant trends. Indeed, for dry northeasterly winds, trends in HWE were remarkably similar to trends in night-time strengthening easterlies over the Sierra Nevada Mountains (compare Figure 2p with Figure S8b), indicating that dry northeasterly winds substantially contribute to the trends seen in Figures 1c,d in this region. Similarly, trends in time series of the average number of Hazardous Wind Events were only positive when relative humidity was considered (Figures S6c,S7c, and 8c), further indicating the importance of drying in the number of HWE. Hence, increasing winds over the Sierra Nevada Mountains are consistent with increases in HWE, but are also substantially driven by drying.

3.4 Trends in Wildfire Conditions

To put wind trends in the context of changing wildfire risk, we examined trends in 2-m temperature, 2-m relative humidity, and the Canadian Fire Weather Index during SON (Figure 4). Daily maximum 2-m temperature increased across almost all of California, and prominently within the Central Valley, the the Sierra Nevada Mountains, and coastal Southern California (Figure 4a). Warming in these regions was also associated with significant drying (Figure 4b). This pattern of warming and drying corresponds to statistically significant increases in FWI across virtually the entire state, with the largest increases confined to the Sierra Nevada Mountains (Figure 4c). Given the concurrent trends in wind speed and HWE in this region, it seems likely that strengthening winds, in addition to warming and drying, have contributed to heightened fire risk over the Sierra Nevada, yet their relative contribution to FWI trends remains to be quantified. Although such an analysis is forgone here, we find that seasonally averaged winds show moderate correlation with seasonally averaged FWI during JJA, especially over the Sierra Nevada (Figure S9), suggesting wind speeds may make a larger contribution to FWI during summer.

Further to the heightened fire risk over the Sierra Nevada, we examined two quantities for the entire state: the daily 90th percentile of Extreme Fire Weather Indices (where extreme FWI are those exceeding 30) and the daily fraction of California covered by these indices. Averaging indices in bins of five successive autumns over 1979–2018 (i.e., 1979–1983, 1984–1988 etc.) shows increasing trends in both quantities (Figure 4d). That is, more of California has become exposed to extreme wildfire risk, increasing from 45% of the state over 1979–1983 to 58% over 2014–2018, with differences in sequential 5-year averages statistically significant from 1989–1993 onward (Table S3). Hence, while fire risk is increasing most over the Sierra Nevada Mountains, California as a whole is also becoming increasingly exposed to extreme wildfire conditions.

4 Conclusions

We examined summer and autumn surface wind trends over California in the ERA5 reanalysis during 1979–2019. The most prominent fire-related trends identified here were in statistically significant increasing easterlies on the western slopes of the Sierra Nevada Mountains that were associated with a 3.1% increase in 95th percentile wind speeds. Associated with these increased wind speeds, we also found statistically significant increases in Hazardous Wind Events of strong, dry, northeasterly winds over the Sierra Nevada Mountains, however drying also appears to be a substantial contributor to the trend. Wind trends also indicated a stronger diurnal circulation over the Sierra Nevada Mountains where the mountains are steepest in the south of the range, with strengthening upslope westerlies during the day and strengthening downslope easterlies at night. This aspect requires further investigation and will be the topic of future work. Indeed, given the many factors that influence wind trends (e.g., changes in regional circulation patterns, land use, surface roughness, observations and assimilation errors (Ramon et al., 2019), an attribution analysis of the trends found here is beyond the scope of this study. Nevertheless, wind trends identified here indicated an increased risk of wind-driven wildfires in a region with a growing wildland-urban interface.

Drawing from time series of seasonally averaged maximum winds historically fire prone region, we also found that while wind speeds have not changed drastically over the past 41 years, there has been a modest shift towards above-average autumn maximum winds over Northern California and the Sierra Nevada Mountains since the early 2000s. While wind speed trends were not statistically significant for Southern California, the region experienced six consecutive summers of above-average maximum wind speeds during 2014–2019 and five consecutive autumns of above-average maximum wind speeds during 2015–2019, coinciding with multiple record-breaking wind-driven wildfires.

Finally, wind trends were put in the context of California's changing wildfire landscape by analyzing trends in the Canadian Fire Weather Index. We found that California has been exposed to increasingly extreme indices over the period of study, increasing from an average of 45% of the state during 1979–1984 to 58% during 2014–2018. Furthermore, autumn fire weather trends have increased greatest and significantly over the Sierra Nevada Mountains where significantly strengthening winds and more frequent Hazardous Wind Events were identified. We therefore propose that surface winds have contributed to increased wildfire risk over the Sierra Nevada Mountains, making them more susceptible to wind-driven wildfires compared to 40 years ago.

Acknowledgments

This research was funded by the University of California Laboratory Fees Research Program (LFR-20-652467) 'Mitigating and Managing Extreme Wildfire Risk in California' project. ATT acknowledges funding from the NSF Grant 2003205, the USDA National Institute of Food and Agriculture, Agricultural and Food Research Initiative Competitive Programme Grant No. 2018-67012-31496. Charles Jones and Leila M. V. Carvalho acknowledge funding from NSF Awards (AGS 1921595, ICER 1664173). The authors would like to acknowledge the high-performance computing support from the NCAR's Computational and Information Systems Laboratory, sponsored by the National Science Foundation. The ERA5 reanalysis data used in this study, as described in Hersbach et al. (2020), is available at https://www.ecmwf.int/en/forecasts/datasets/reanalysis-datasets/era5,

and the ERA5-based Canadian Fire Weather Index data, as described in Vitolo et al. (2020), is available at https://cds.climate.copernicus.eu/cdsapp#!/dataset/cems-fire-historical?tab=overview.

References

Abatzoglou, J. T., Barbero, R., & Nauslar, N. J. (2013). Diagnosing Santa Ana winds in Southern California with synoptic-scale analysis. *Weather and Forecasting*, *28*, 704-710. doi: 10.1175/WAF-D-13-00002.1

Abatzoglou, J. T., Smith, C. M., Swain, D. L., Ptak, T., & Kolden, C. A. (2020). Population exposure to pre-emptive deenergization aimed at averting wildfires in Northern California. *Environmental Research Letters*, *15*. doi: 10.1088/1748-9326/aba135

Alizadeh, M. R., Abatzoglou, J. T., Luce, C. H., Adamowski, J. F., Farid, A., & Sadegh, M. (2021). Warming enabled upslope advance in western US forest fires. *Proceedings of the National Academy of Sciences*, *118*. doi: 10.1073/pnas.2009717118

Bosart, L. F. (1983). Analysis of a California Catalina Eddy event. *Monthly Weather Review*, *111*, 1619–1633. doi: 10.1175/1520-0493(1983)111⟨1619:AOACCE⟩2.0.CO;2

Brewer, M. J., & Clements, C. B. (2020). The 2018 Camp Fire: Meteorological analysis using in situ observations and numerical simulations. *Atmosphere*, *11*. doi: 10.3390/atmos11010047

CalFire. (2020a). Top 20 Deadliest California Wildfires. `https://www.fire.ca.gov/media/5512/top20_deadliest.pdf`. (Accessed: 19/10/2020)

CalFire. (2020b). Top 20 Largest California Wildfires. `https://www.fire.ca.gov/media/11416/top20\_acres.pdf`. (Accessed: 19/10/2020)

Carvalho, L., Duine, G.-J., Jones, C., Zigner, K., Clements, C., Kane, H., … Enos, W. (2020). The Sundowner Winds Experiment (SWEX) Pilot Study: Understanding downslope windstorms in the Santa Ynez mountains, Santa Barbara, California. *Monthly Weather Review*, *148*, 1519 - 1539. doi: 10.1175/MWR-D-19-0207.1

Coen, J. L., Schroeder, W., & Quayle, B. (2018). The generation and forecast of extreme winds during the origin and progression of the 2017 Tubbs Fire. *Atmosphere*, *9*. doi: 10.3390/atmos9120462

Duine, G.-J., Jones, C., Carvalho, L. M., & Fovell, R. G. (2019). Simulating Sundowner winds in coastal Santa Barbara: Model validation and sensitivity. *Atmosphere*, *10*. doi: 10.3390/atmos10030155

Field, R. D., Spessa, A. C., Aziz, N. A., Camia, A., Cantin, A., Carr, R., . . . Wang, X. (2015). Development of a global fire weather database. *Natural Hazards and Earth System Sciences*, *15*, 1407–1423. doi: 10.5194/nhess-15-1407-2015

Fovell, R. G., & Gallagher, A. (2018). Winds and gusts during the Thomas Fire. *Fire*, *1*(3). doi: 10.3390/fire1030047

Goss, M., Swain, D. L., Abatzoglou, J. T., Sarhadi, A., Kolden, C. A., Williams, A. P., & Diffenbaugh, N. S. (2020). Climate change is increasing the likelihood of extreme autumn wildfire conditions across California. *Environmental Research Letters*, *15*, pp.14. doi: 10.1088/1748-9326/ab83a7

Guzman-Morales, J., & Gershunov, A. (2019). Climate change suppresses Santa Ana winds of Southern California and sharpens their seasonality. *Geophysical Research Letters*, *46*, 2772–2780. doi: 10.1029/2018GL080261

Guzman-Morales, J., Gershunov, A., Theiss, J., Li, H., & Cayan, D. (2016). Santa Ana winds of Southern California: Their climatology, extremes, and behavior spanning six and a half decades. *Geophysical Research Letters*, *43*, 2827-2834. doi: https://doi.org/10.1002/2016GL067887

Hammer Roger B., F. J. S., Radeloff Volker C., & I., S. S. (2007). Wildland–urban interface housing growth during the 1990s in California, Oregon, and Washington. *International Journal of Wildland Fire*, *16*, 255-265. doi: https://doi.org/10.1071/WF05077

Hatchett, B. J., Smith, C. M., Nauslar, N. J., & Kaplan, M. L. (2018). Brief communication: Synoptic-scale differences between Sundowner and Santa Ana wind regimes in the Santa Ynez Mountains, California. *Natural Hazards and Earth System Sciences*, *18*, 419–427. doi: 10.5194/nhess-18-419-2018

Hayhoe, K., Cayan, D., Field, C. B., Frumhoff, P. C., Maurer, E. P., Miller, N. L., . . . Verville, J. H. (2004). Emissions pathways, climate change, and impacts on California. *Proceedings of the National Academy of Sciences*, *101*, 12422–12427. doi: 10.1073/pnas.0404500101

Hersbach, H., Bell, B., Berrisford, P., Hirahara, S., Horányi, A., Muñoz-Sabater, J., . . . Thépaut, J.-N. (2020). The ERA5 global reanalysis. *Quarterly Journal of* *the Royal Meteorological Society*, *146*, 1999–2049. doi: 10.1002/qj.3803

Holt, E., & Wang, J. (2012). Trends in wind speed at wind turbine height of 80 m over the contiguous United States using the North American Regional Reanalysis (NARR). *Journal of Applied Meteorology and Climatology*, *51*, 2188–2202. doi: 10.1175/JAMC-D-11-0205.1

Hughes, M., Hall, A., & Kim, J. (2011). Human-induced changes in wind, temperature and relative humidity during Santa Ana events. *Climatic Change*, *109*, 1573–1480. doi: 10.1007/s10584-011-0300-9

Jones, C., Carvalho, L. M., Duine, G.-J., & Zigner, K. (2021). Climatology of Sundowner winds in coastal Santa Barbara, California, based on 30 yr high resolution WRF downscaling. *Atmospheric Research*, *249*. doi: https://doi.org/10.1016/j.atmosres.2020.105305

Jones, C., Fujioka, F., & Carvalho, L. M. V. (2010). Forecast skill of synoptic conditions associated with Santa Ana winds in Southern California. *Monthly Weather Review*, *138*, 4528–4541. doi: 10.1175/2010MWR3406.1

Jourdier, B. (2020). Evaluation of ERA5, MERRA-2, COSMO-REA6, NEWA and AROME to simulate wind power production over France. *Advances in Science and Research*, *17*, 63–77. doi: 10.5194/asr-17-63-2020

Kanamitsu, M., Yulaeva, E., Li, H., & Hong, S.-Y. (2013). Catalina Eddy as revealed by the historical downscaling of reanalysis. *Asia-Pacific Journal of the Atmospheric Sciences*, *49*, 467-481. doi: 10.1007/s13143-013-0042-x

Kolden, C. A., & Henson, C. (2019). A socio-ecological approach to mitigating wildfire vulnerability in the wildland urban interface: A case study from the 2017 thomas fire. *Fire*, *2*. doi: 10.3390/fire2010009

Letcher, T., & Minder, J. (2017a, 12). The simulated impact of the snow albedo feedback on the large-scale mountain–plain circulation east of the Colorado Rocky Mountains. *Journal of the Atmospheric Sciences*, *75*, 755–774. doi: 10.1175/JAS-D-17-0166.1

Letcher, T., & Minder, J. (2017b, 09). The simulated response of diurnal mountain winds to regionally enhanced warming caused by the snow albedo feedback. *Journal of the Atmospheric Sciences*, *74*, 49-67. doi: 10.1175/JAS-D-16-0158.1

Li, A. K., Paek, H., & Yu, J.-Y. (2016). The changing influences of the AMO and PDO on the decadal variation of the Santa Ana winds. *Environmental Research Letters*, *11*. doi: 10.1088/1748-9326/11/6/064019

Liu, Y.-C., Di, P., Chen, S.-H., Chen, X., Fan, J., DaMassa, J., & Avise, J. (2020). Climatology of Diablo winds in Northern California and their relationships with large-scale climate variabilities. *Climate Dynamics*. doi: 10.1007/s00382-020-05535-5

Mass, C. F., & Ovens, D. (2021). The synoptic and mesoscale evolution accompanying the 2018 Camp Fire of Northern California. *Bulletin of the American Meteorological Society*, *102*, 168 - 192. doi: 10.1175/BAMS-D-20-0124.1

Miller, N. L., & Schlegel, N. J. (2006). Climate change projected fire weather sensitivity: California Santa Ana wind occurrence. *Geophysical Research Letters*, *33*. doi: 10.1029/2006GL025808

Mitchell, J. W. (2013). Power line failures and catastrophic wildfires under extreme weather conditions. *Engineering Failure Analysis*, *35*, 726-735. doi: https://doi.org/10.1016/j.engfailanal.2013.07.006

Nauslar, N. J., Abatzoglou, J. T., & Marsh, P. T. (2018). The 2017 North Bay and Southern California fires: A case study. *Fire*, *1*. doi: 10.3390/fire1010018

Norris, C. L. M. V. J. C., Jesse, & Cannon, F. (2020). Warming and drying over the central Himalaya caused by an amplification of local mountain circulation. *npj Climate and Atmospheric Science*, *33*. doi: https://doi.org/10.1038/s41612-019-0105-5

OES. (2018). 2018 California State Hazard and Mitigation Plan. `https://www.caloes.ca.gov/cal-oes-divisions/hazard-mitigation/hazard-mitigation-planning/state-hazard-mitigation-plan`. (Accessed: 19/10/2020)

Ramon, J., Lledó, L., Torralba, V., Soret, A., & Doblas-Reyes, F. J. (2019). What global reanalysis best represents near-surface winds? *Quarterly Journal of the Royal Meteorological Society*, *145*, 3236–3251. doi: 10.1002/qj.3616

Rolinski, T., Capps, S. B., & Zhuang, W. (2019). Santa Ana winds: A descriptive climatology. *Weather and Forecasting*, *34*, 257–275. doi: 10.1175/WAF-D-18-0160.1

Schwartz, M. W., Butt, N., Dolanc, C. R., Holguin, A., Moritz, M. A., North, M. P., . . . van Mantgem, P. J. (2015). Increasing elevation of fire in the Sierra Nevada and implications for forest change. *Ecosphere*, *6*. doi: https://doi.org/10.1890/ES15-00003.1

Thompson, W. T., Burk, S. D., & Rosenthal, J. (1997). An investigation of the Catalina Eddy. *Monthly Weather Review*, *125*, 1135 - 1146. doi: 10.1175/1520-0493(1997)125⟨1135:AIOTCE⟩2.0.CO;2

Vitolo, C., Di Giuseppe, F., Barnard, C., Coughlan, R., San-Miguel-Ayanz, J., Libertá, G., & Krzeminski, B. (2020). ERA5-based global meteorological wildfire danger maps. *Scientific Data*, *7*, 2052–4463. doi: 10.1038/s41597-020-0554-z

Werth, P. A., Potter, B. E., Alexander, M. E., Clements, C. B., Cruz, M. G., Finney, M. A., ... Parsons, R. A. (2016). *Synthesis of knowledge of extreme fire behavior: Volume 2 for fire behavior specialists, researchers, and meteorologists.* U.S. Department of Agriculture, Forest Service.

Westerling, A. L., Hidalgo, H. G., Cayan, D. R., & Swetnam, T. W. (2006). Warming and earlier spring increase western U.S. forest wildfire activity. *Science*, *313*, 940–943. doi: 10.1126/science.1128834

Wilks, D. S. (2011). *Statistical methods in the atmospheric sciences* (Third Edition ed.). Academic Press.

Williams, A. P., Abatzoglou, J. T., Gershunov, A., Guzman-Morales, J., Bishop, D. A., Balch, J. K., & Lettenmaier, D. P. (2019). Observed impacts of anthropogenic climate change on wildfire in California. *Earth's Future*, *7*, 892–910. doi: 10.1029/2019EF001210

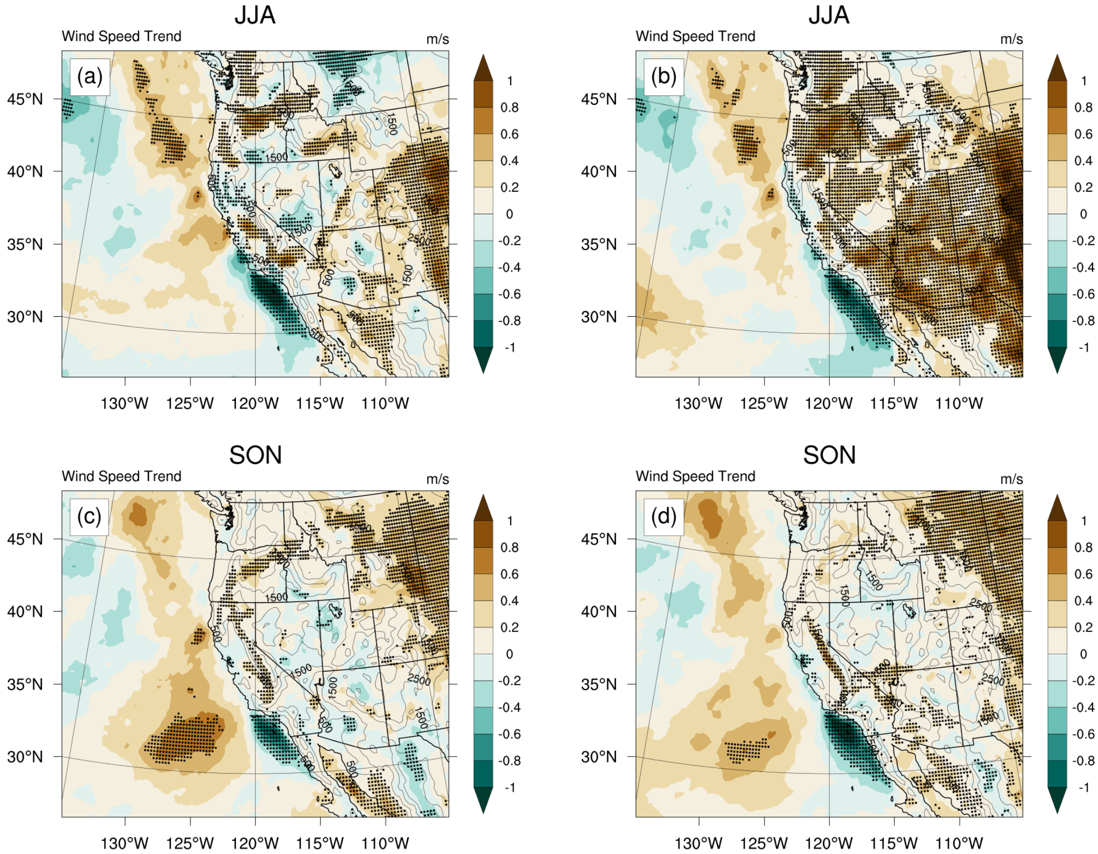

Figure 1. Trends in seasonally averaged daytime (0600–1700 PST) maximum 10-m wind speed for JJA (a) and SON (b) and seasonally averaged night-time (1800–0500 PST) maximum 10-m wind speed for JJA (c) and SON (d) during 1979–2019. Solid colors denote the wind speed trend which has been multiplied by the total number of years during 1979–2019 to highlight the total change. Dots indicate statistically significant trends at the 95% level from Mann-Kendall testing. Black contours show the ERA5 orography.

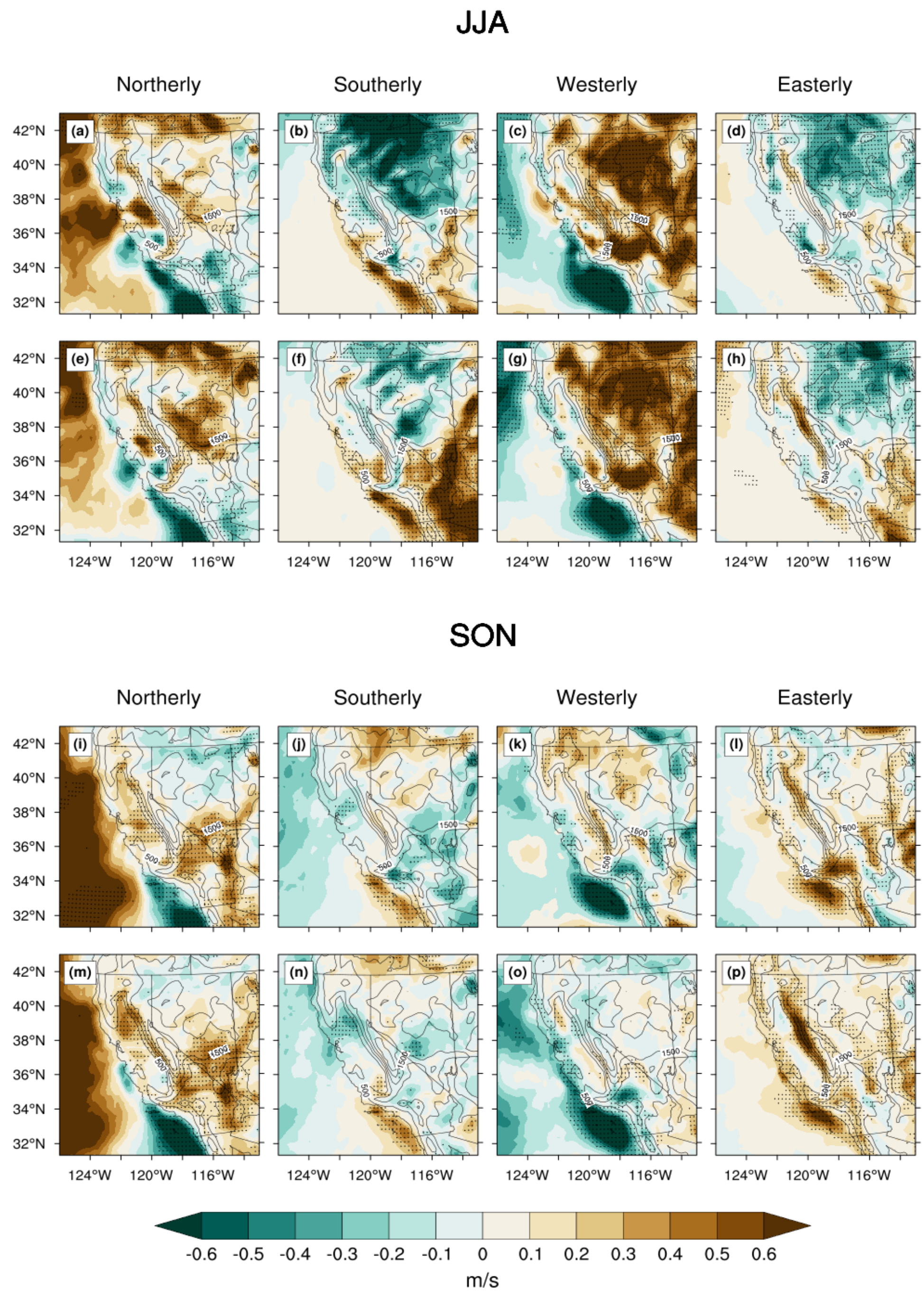

Figure 2. Trends in seasonally averaged daily maximum northerly and westerly winds and trends in seasonally averaged daily minimum southerly and easterly winds during the day (0600–1700 PST) and at night (1800–0500 PST) during JJA and SON. The top set of panels shows JJA trends for daytime (night-time) northerlies, southerlies, westerlies and easterlies in subplots a–d (e–h). Similarly, the bottom set of panels shows SON trends for daytime (night-time) northerlies, southerlies, westerlies and easterlies in subplots i–l (m–p). Trends have been multiplied by the total number of years during 1979-2019 to highlight the total change. As northerly and easterly winds in ERA5 are traditionally negative, northerly and easterly wind trends are multiplied by –1 so that in all subplots brown colors indicate strengthening winds and blue colors indicate weakening winds.

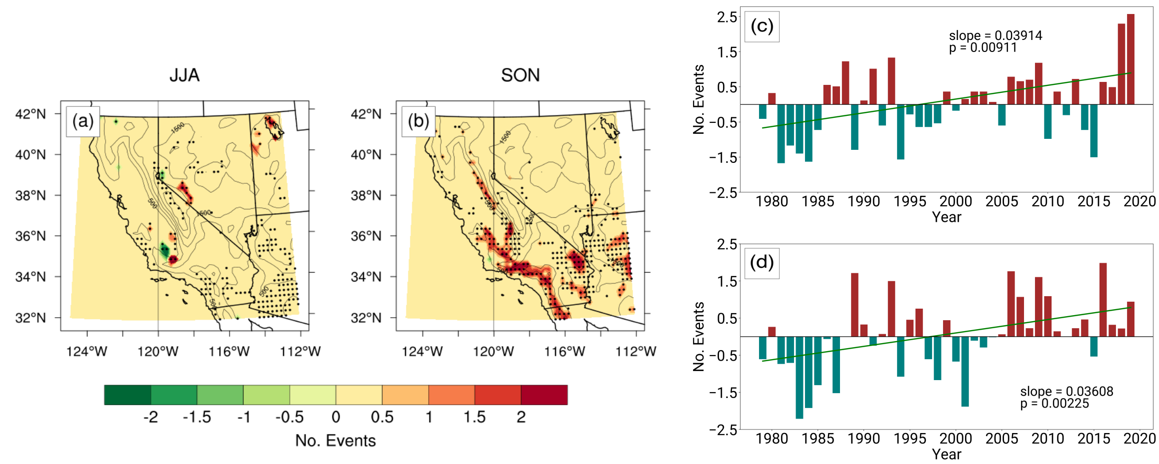

Figure 3. Left horizontal panels show trends in the number of Hazardous Wind Events during JJA (a) and SON (b) during 1979–2019 (solid colors). Trends have been multiplied by the total number of years during 1979–2019 to highlight the total change. Black dots indicate statistically significant trends at the 95% significance level. Black contours show ERA5 orography. Right vertical panels show time series and trends in the standardized number of Hazardous Wind Events during SON over the Sierra Nevada Mountains (c) (36.25–38.5 N and 117.5–120 W) and Southern California (d) (32.7–35 N and 115–119 W). Time series entries were calculated by averaging the number of Hazardous Wind Events during SON in each region. Time series were then standardized by subtracting their mean and dividing by their standard deviation. Green lines denote the Theil-Sen trends.

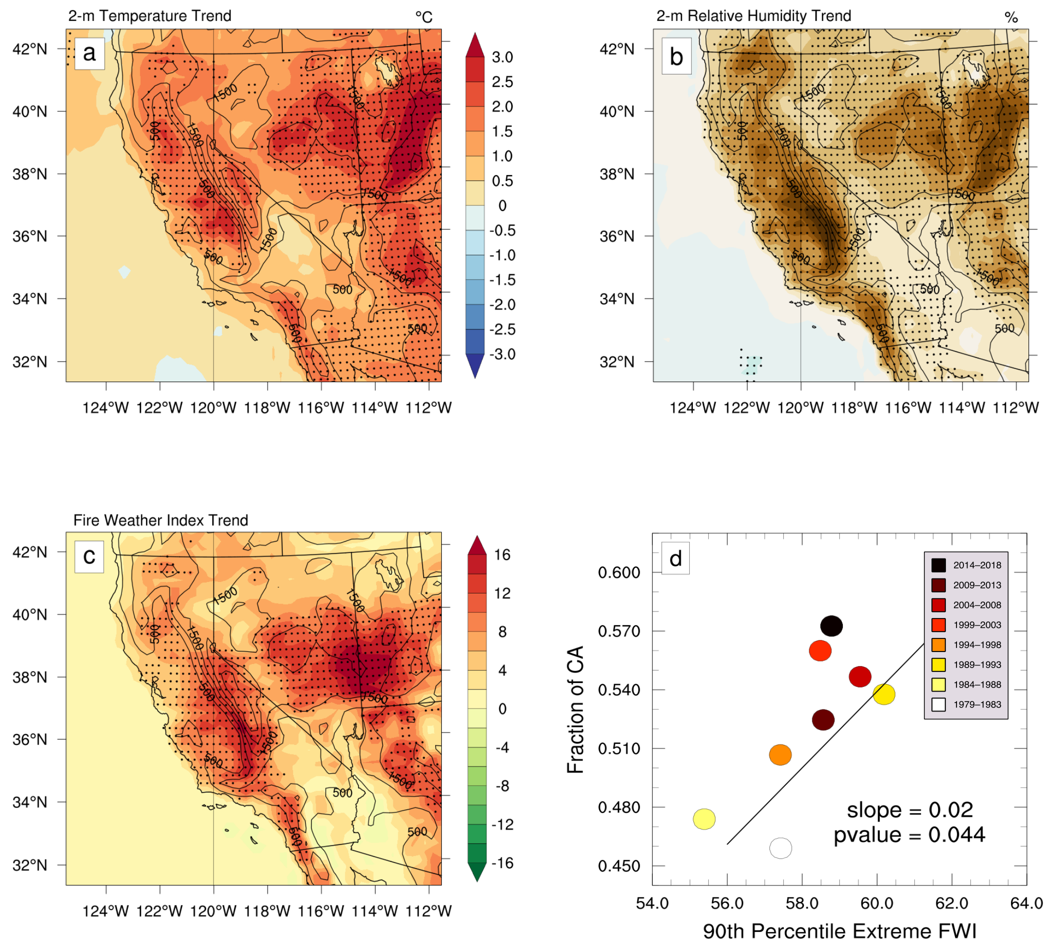

Figure 4. Trends during SON over 1979–2019 in (a) daily maximum 2-meter temperature, (b) daily minimum 1000-hPa relative humidity, (c) Canadian Fire-Weather Index (FWI), and (d) 5-year SON averages in the fraction of California covered by Extreme FWIs vs 5-year SON averages of daily 90th percentile Extreme FWI. Trends have been multiplied by the total number of years during 1979–2019 to highlight the total change. Dots in (a), (b), and (c) indicate statistically significant trends at the 95% significance level under Mann-Kendall testing. Markers in (d) tend from the bottom left quadrant towards the top right quadrant as one moves from lighter to darker shades (i.e., from the 1979–1983 toward 2014–2018), indicating increased and more widespread wildfire risk.

Supporting Information for 'Increasing Wind-Driven Wildfire Risk Across California's Sierra Nevada Mountains'

Callum Thompson[1], Charles Jones[1,2], Leila Carvalho[1,2], Anna Trugman[1,2],

Donald D. Lucas[3], Daisuke Seto[1] and Kevin Varga[1]

[1]Earth Research Institute, University of California Santa Barbara

[2]Department of Geography, University of California Santa Barbara

[3]Lawrence Livermore National Laboratory

Contents of this file

Top 20 Largest California Wildfires					
Fire Name (Cause)	Date	County	Acres	Structures	Deaths
AUGUST COMPLEX (Under Investigation)*	August 2020	Mendocino, Humboldt, Trinity, Tehama, Glenn & Colusa	1,032,649	935	1
MENDOCINO COMPLEX (Under Investigation)	July 2018	Colusa, Lake, Mendocino & Glenn	459,123	280	1
SCU LIGHTNING COMPLEX (Under Investigation)*	August 2020	Stanislaus, Santa Clara, Alameda, Contra Costa & San Joaquin	396,624	222	0
CREEK FIRE (Under Investigation)*	September 2020	Fresno & Madera	377,693	853	0
LNU LIGHTNING COMPLEX (Under Investigation)*	August 2020	Sonoma, Lake, Napa, Yolo, & Solano	363,220	1,491	6
NORTH COMPLEX (Under Investigation)*	August 2020	Butte, Plumas, & Yuba	318,930	2,352	15
THOMAS (Powerlines)	December 2017	Ventura & Santa Barbara	281,893	1,063	2
CEDAR (Human Related)	October 2003	San Diego	273,246	2,820	15
RUSH (Lightning)	August 2012	Lassen	271,911 CA / 43,666 NV	0	0
RIM (Human Related)	August 2013	Tuolumne	257,314	112	0
ZACA (Human Related)	July 2007	Santa Barbara	240,207	1	0
CARR (Human Related)	July 2018	Shasta County & Trinity	229,651	1,614	8
MATILIJA (Undetermined)	September 1932	Ventura	220,000	0	0
WITCH (Powerlines)	October 2007	San Diego	197,990	1,650	2
KLAMATH THEATER COMPLEX (Lightning)	June 2008	Siskiyou	192,038	0	2
MARBLE CONE (Lightning)	July 1977	Monterey	177,866	0	0
LAGUNA (Powerlines)	September 1970	San Diego	175,425	382	5
SQF Complex (Lightning)	August 2020	Tulare	170,384	228	0
BASIN Complex (Lightning)	June 2008	Monterey	162,818	58	0
DAY FIRE (Human Related)	September 2006	Ventura	162,702	11	0

Table S1. Top 20 Largest California Wildfires as of 19 October 2020 according to the California Department of Forestry and Fire Protection (CAL FIRE): https://www.fire.ca.gov/media/11416/top20_acres.pdf. Astericks indicate numbers are not final.

Top 20 Deadliest California Wildfires					
Fire Name (Cause)	Date	County	Acres	Structures	Deaths
CAMP FIRE (Powerlines)	November 2018	Butte	153,336	18,804	85
GRIFFITH PARK (Unknown)	October 1933	Los Angeles	47	0	29
TUNNEL - OAKLAND HILLS (Rekindle)	October 1991	Alameda	1,600	2,900	25
TUBBS (Electrical)	October 2017	Napa & Sonoma	36,807	5,643	22
NORTH COMPLEX (Under Investigation)*	August 2020	Butte, Plumas, & Yuba	318,935	2,352	15
CEDAR (Human Related)	October 2003	San Diego	273,246	2,820	15
RATTLESNAKE (Arson)	July 1953	Glenn	1,340	0	15
LOOP (Unknown)	November 1966	Los Angeles	2,028	0	12
HAUSER CREEK (Human Related)	October 1943	San Diego	13,145	0	11
INAJA (Human Related)	November 1956	San Diego	43,904	0	11
IRON ALPS COMPLEX (Lightning)	August 2008	Trinity	105,855	10	10
REDWOOD VALLEY (Power Lines)	October 2017	Mendocino	36,523	544	9
HARRIS (Undetermined)	October 2007	San Diego	90,440	548	8
CANYON (Unknown)	August 1968	Los Angeles	22,197	0	8
CARR (Human Related)	July 2018	Shasta County, Trinity	229,651	1,614	8
LNU Lightning Complex (Under Investigation)*	August 2020	Napa/Sonoma/Yolo/Stanislaus/ Lake	363,220	1,491	6
ATLAS (Powerline)	October 2017	Napa & Solano	51,624	781	6
OLD (Human Related)	October 2003	San Bernardino	91,281	1,003	6
DECKER (Vehicle)	August 1959	Riverside	1,425	1	6
HACIENDA (Unknown)	September 1955	Los Angeles	1,150	0	6

Table S2. Top 20 Deadliest California Wildfires as of 19 October 2020 according to the California Department of Forestry and Fire Protection (CAL FIRE): https://www.fire.ca284.gov/media/5512/top20_deadliest.pdf. Astericks indicate numbers are not final.

SON	1979-1983	1984-1988	1989-1993	1994-1998	1999-2003	2004-2008	2009-2013	2014-2018
1979-1983	1	0.3472	0	0.02	0	0	0	0
1984-1988	0.3472	1	0.0001	0.0386	0	0	0.0019	0
1989-1993	0	0.0001	1	0.043	0.1604	0.5759	0.4049	0.0215
1994-1998	0.002	0.0386	0.043	1	0.0009	0.0141	0.2606	0
1999-2003	0	0	0.1604	0.0009	1	0.43	0.0319	0.4291
2004-2008	0	0	0.5759	0.0141	0.43	1	0.1856	0.1088
2009-2013	0	0.0019	0.4049	0.2606	0.0319	0.1856	1	0.0024
2014-2018	0	0	0.0215	0	0.4291	0.1088	0.0024	1

Table S3. P-values for Student t-tests on the difference in 5-year SON statewide averages of the Canadian Fire Weather Index between 1979-1983 and 2014-2018 in Figure 4d.

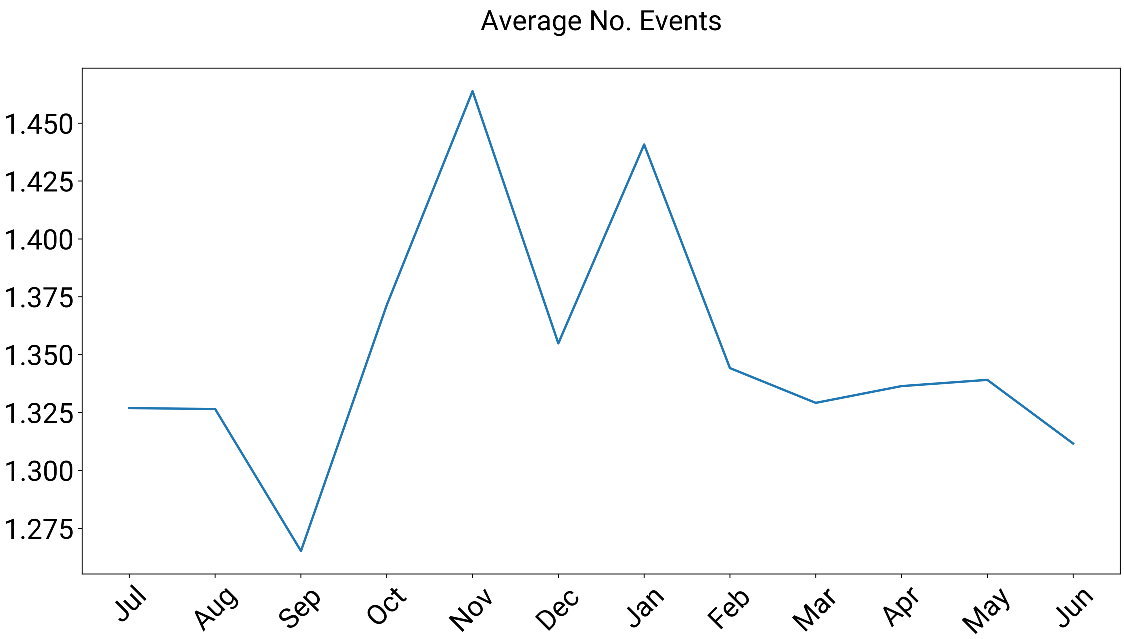

Figure S1. Monthly average number of Hazardous Wind Events within California over 1979-2019.

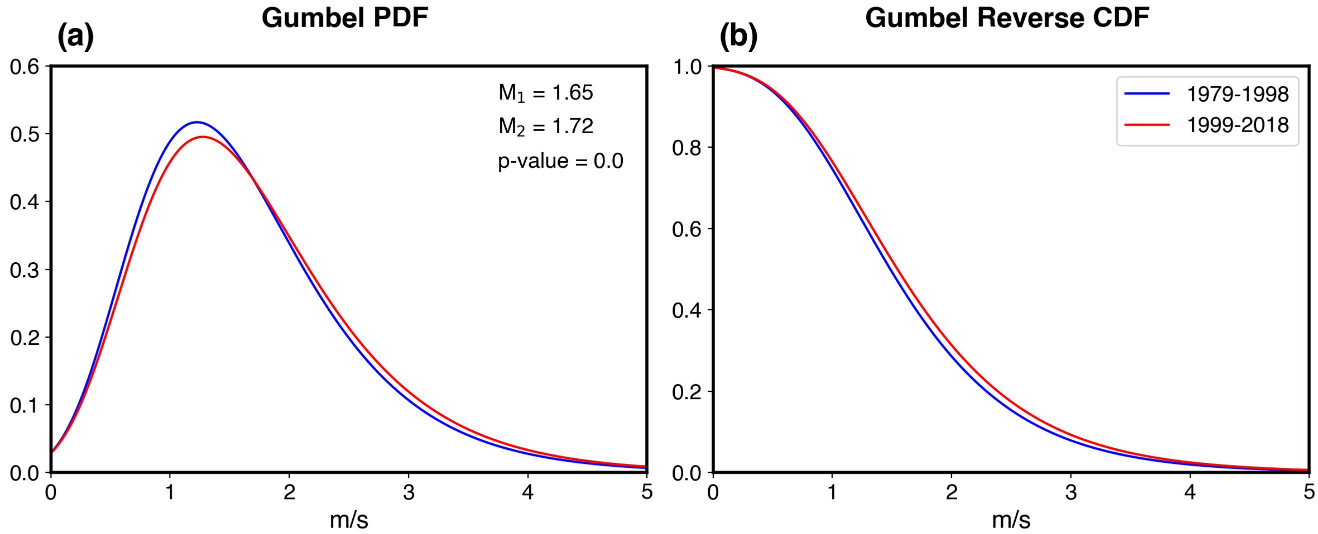

Figure S2. Fitted Gumbel probability distribution function (a) and reversed cumulative distribution function (b) of SON wind speeds at statistically significant grid points over the Sierra Nevada Mountains (38.5–36.25 N and 117.5–120.5 W) during 1979–1998 (blue) and 1999–2018 (red). M1 and M2 denote the 1979–1998 and 1999–2018 distributions means, respectively. The p-value corresponds to a one sided t-test for identical sample means.

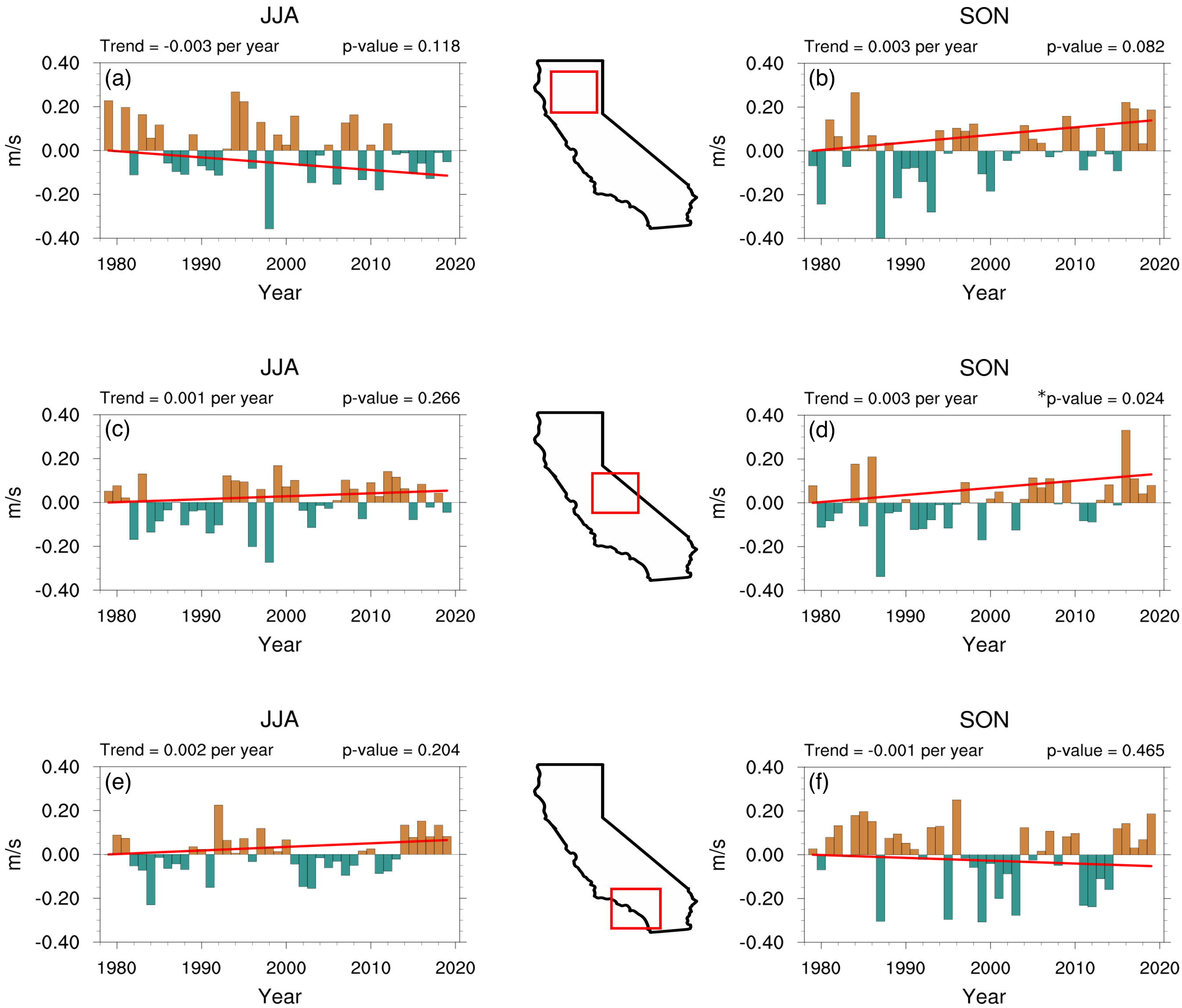

Figure S3. Anomalies in seasonally averages of daily maximum winds by region for JJA (left column) and SON (right column) over 1979–2019. Years of above average and below average maximum wind speeds are colored in brown and teal, respectively. Corresponding Theil-Sen linear trends (red lines) and their Mann-Kendall test p-values are annotated on the top left and top right of each subplot, respectively. Red boxes represent the three target regions of interest defined in the text.

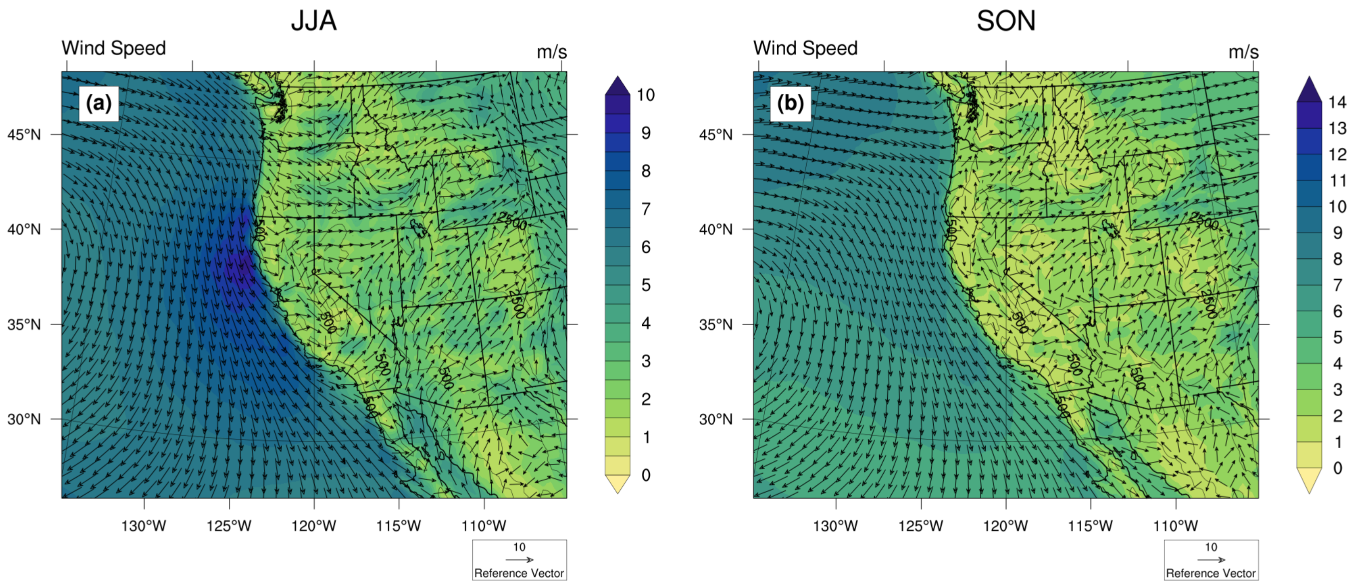

Figure S4. Seasonal average ERA5 10-m wind speed (solid colors) and seasonal average zonal and meridional wind components (arrows) for JJA (a) and SON (b) over 1979–2019. Note the different color bars for each subplot.

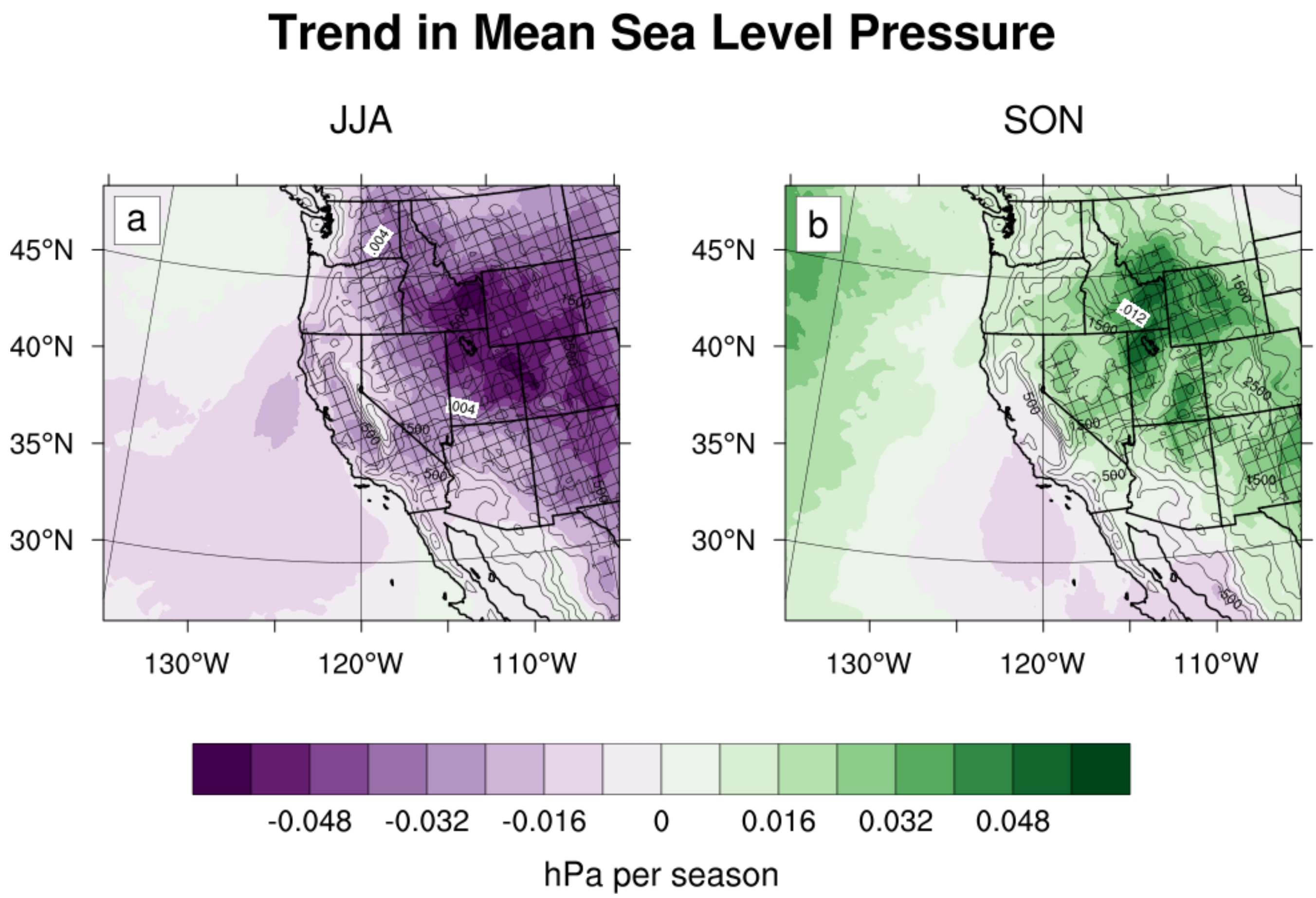

Figure S5. Trend in seasonally averaged mean sea level pressure (solid colors) over 1979–2019 for JJA (a) and SON (b). Hatching denotes statistical significant trends at the 95% significance level from Mann-Kendall testing. Black contours show ERA5 orography.

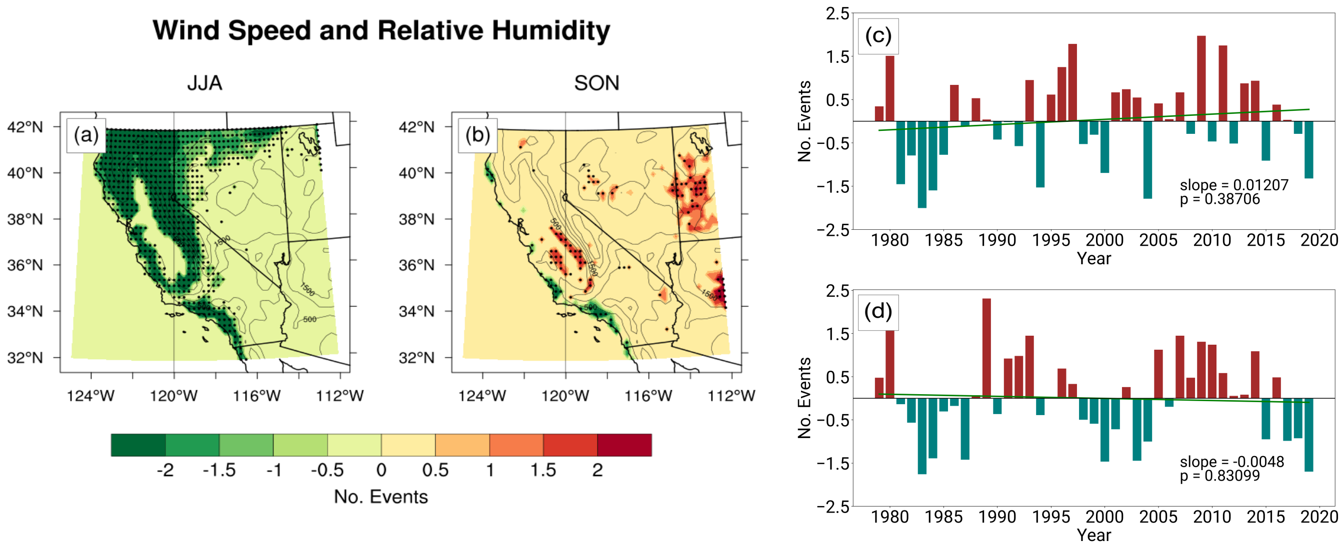

Figure S6. Left horizontal panels show trends in the number of strong, dry wind events during JJA (a) and SON (b) (solid colors). Black dots indicate statistically significant trends at the 95% significance level. Black contours show ERA5 orography. Right vertical panels show trends in the standardized number of Hazardous Wind Events during SON for the Sierra Nevada Mountains (c) and Southern California (d). Time series entries were calculated by averaging the number of Hazardous Wind Events during SON for each year during 1979–2019. Time series were then standardized by subtracting its mean and dividing by its standard deviation. Green lines denote the Theil-Sen trends.

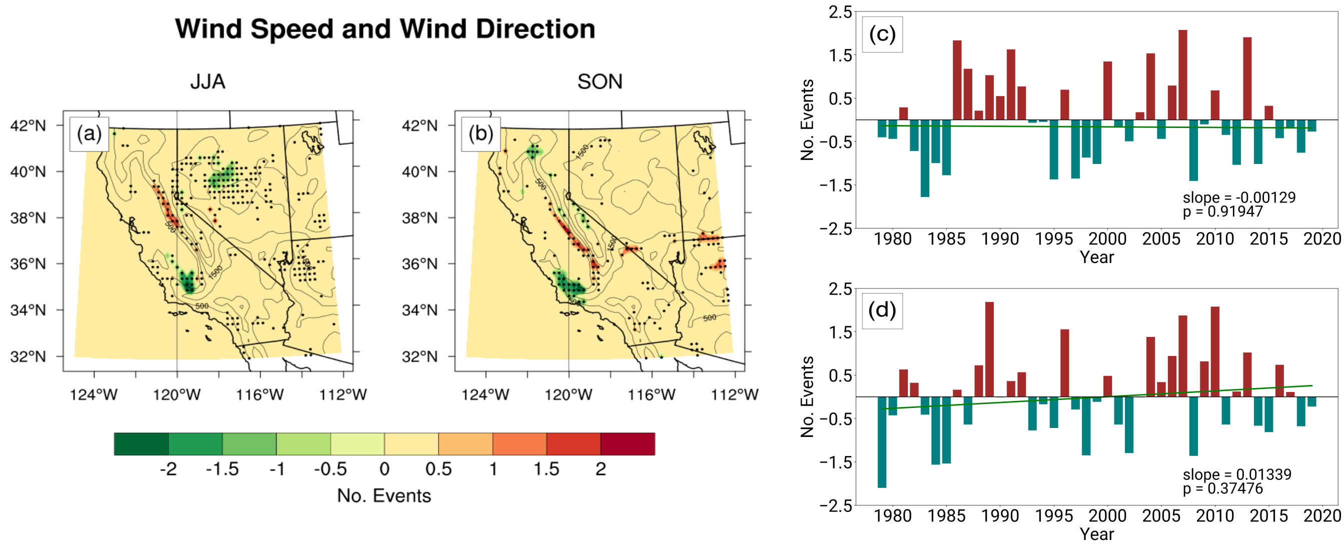

Figure S7. As in Figure S6, but for strong, northeasterly wind events.

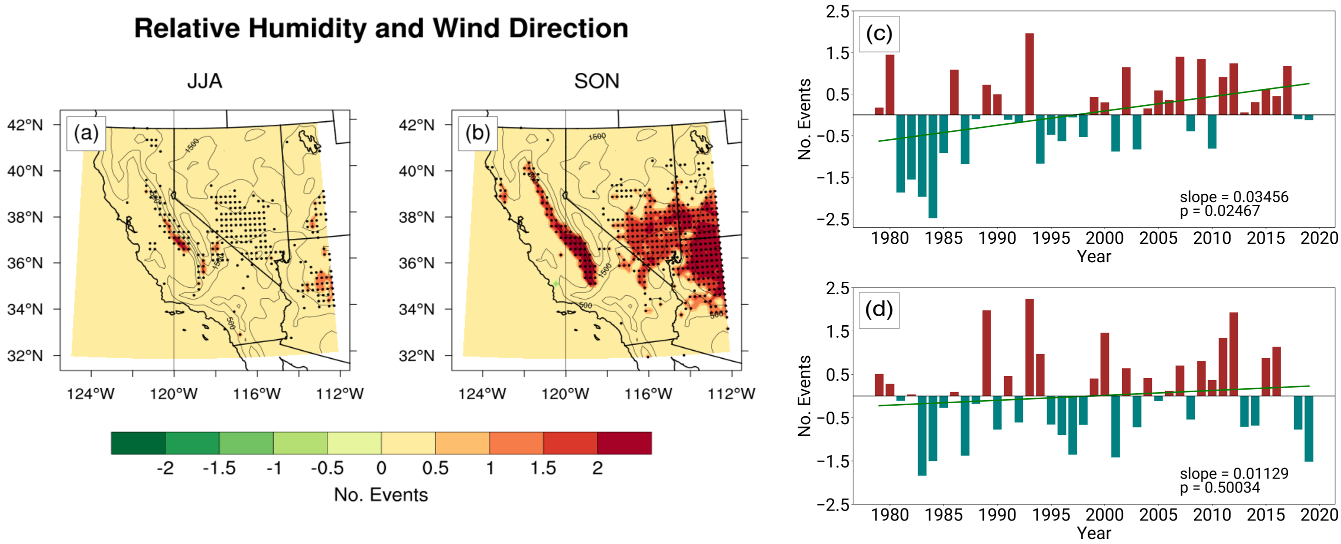

Figure S8. As in Figure S6, but for dry, northeasterly wind events.

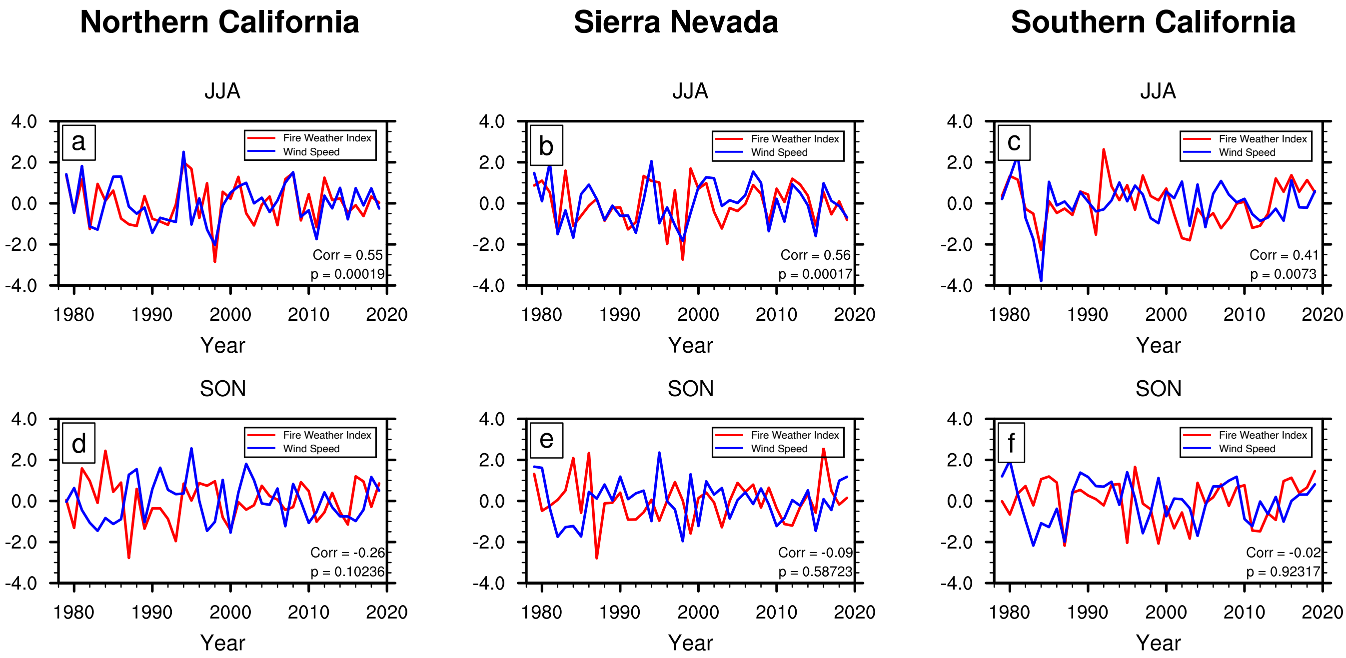

Figure S9. Seasonal average 10-m wind speed and seasonal average Fire Weather Index and their Pearson correlation for Northern California (39–41.5 N and 120.5–123.5 W), the Sierra Nevada Mountains (36.25–38.5 N and 117.5–120 W), and Southern California (32.7–35 N and 115–119 W) for JJA (a–c) and SON (d–f) during 1979–2019.